Lawrence Berkeley National Laboratory

Title

Evaluating Possible Formation Mechanisms of Criegee Intermediates during the Heterogeneous Autoxidation of Squalene

Permalink

https://escholarship.org/uc/item/3xw3r7b2

Journal

ISSN

Authors

Zeng, Meirong

Wilson, Kevin R

Publication Date

2024-07-02

DOI

Copyright Information

Peer reviewed

Evaluating Possible Formation Mechanisms of Criegee Intermediates During the Heterogeneous Autoxidation of Squalene

Meirong Zeng [a] and Kevin R. Wilson [b]*

[a] College of Smart Energy, Shanghai Jiao Tong University, Shanghai 200240, PR China
[b] Chemical Sciences Division, Lawrence Berkeley National Laboratory, Berkeley, CA 94720, United States.

Corresponding Author*: Kevin R. Wilson (email: krwilson@lbl.gov)

ABSTRACT

Organic molecules in the environment oxidatively degrade by a variety of free radical, microbial and biogeochemical pathways. A significant pathway is heterogeneous autoxidation, in which degradation occurs via a network of carbon and oxygen centered free radicals. Recently, we found evidence for a new heterogeneous autoxidation mechanism of squalene that is initiated by hydroxyl (OH) radical addition to a carbon-carbon double bond and apparently propagated through pathways involving Criegee Intermediates (CI) produced from β-hydroxy peroxy radicals (β-OH-$RO_2^\bullet$). It remains unclear, however, exactly how CI are formed from β-OH-$RO_2^\bullet$, which could occur by a unimolecular or bimolecular pathway. Combining kinetic models and multiphase OH oxidation measurements of squalene, we evaluate the kinetic viability of three mechanistic scenarios. Scenario 1 assumes that CI are formed by the unimolecular bond scission of β-OH-$RO_2^\bullet$, whereas Scenarios 2 and 3 test bimolecular pathways of β-OH-$RO_2^\bullet$ to yield CI. Scenario 1 best replicates the entire experimental data set, which includes effective uptake coefficients vs. [OH] as well as the formation kinetics of the major products (*i.e.,* aldehydes and secondary ozonides). Although the unimolecular pathway appears to be kinetically viable, future high-level theory is needed to fully explain the mechanistic relationship between CI and β-OH-$RO_2^\bullet$ in the condensed-phase.

KEYWORDS: Autoxidation, Criegee Intermediates, β-Hydroxy peroxy radical, Heterogeneous kinetics, Kinetic modelling

SYNOPSIS: Three kinetic scenarios are evaluated to reveal how Criegee Intermediates propagate the autoxidative degradation of organic molecules in the atmospheric and environment.

1. INTRODUCTION

Reactive oxygen species (ROS), such as the hydroxyl radical (OH), hydroperoxyl radical (HO_2) and hydrogen peroxide (H_2O_2), initiate free radical chain reactions that degrade organic molecules.[1-3] ROS can initiate/propagate chain reactions that lead to the spoilage of food, the degradation of plastics, fuels and cellular membranes, as well as other environmental and petrochemicals. The oxidation of lipid molecules in cellular membranes (known as lipid peroxidation) causes an imbalance between ROS production and antioxidant defenses, which is widely recognized as oxidative stress and thought to be responsible for oxidative aging, cancer, neurodegeneration, diabetes and etc.[1, 4-6] Additionally, evidence has been reported that OH initiated autoxidation accelerates the oxidative transformation organic aerosols in the atmosphere by 2-3 orders of magnitude.[7] This heterogeneous autoxidation mechanism would substantially shorten the lifetime of organic aerosols in the atmosphere with potentially larger scale impacts for predicting how particulate matter impacts air quality, climate and human health.[6, 8-10] Thus, given the importance of oxidation for transforming organic molecules, an in-depth understanding of the overall reaction mechanism that controls autoxidation rates is essential when designing effective antioxidants to prevent cellular damage or for a broader understanding of environmental and atmospheric degradation pathways.

Decades of research has yielded a detailed mechanistic picture of lipid peroxidation.[11, 12] The conventional picture of autoxidation begins with H atom abstraction (*e.g.,* by ROS) at an allylic or bi-allylic site of an organic molecule (RH) to generate the alkyl radical (R•), as illustrated in Fig. 1A. In the presence of O_2 the carbon centered alkyl radical is transformed into a peroxy radical (RO_2•). RO_2• is the key intermediate that propagates the chain reaction in another H-abstraction step to form a hydroperoxide (ROOH). Decomposition of ROOH also contributes to the pool of

free radicals as well as a variety of more volatile scission products that include aldehydes, which are often associated with onset rancidity in foods and toxicity in the environment.
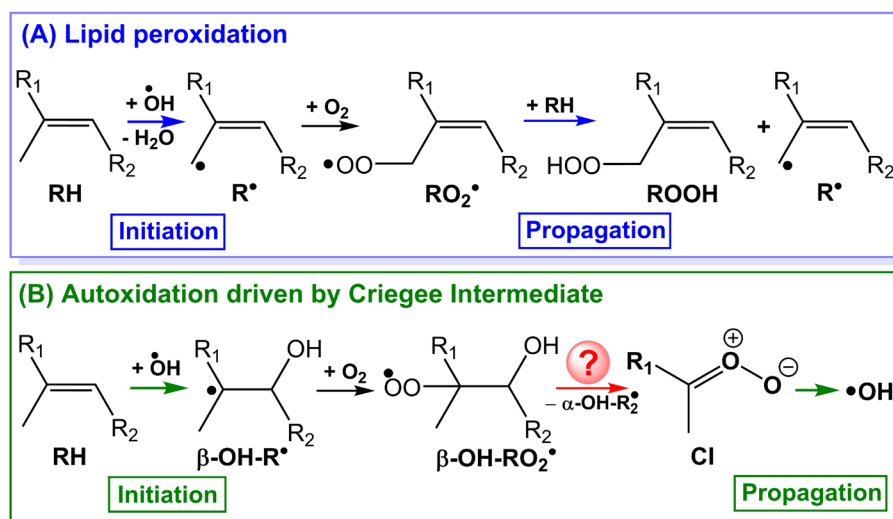
Figure 1. (A) The conventional autoxidation mechanism driven by reactions of peroxy radical $(RO_2^\bullet)$[11] and (B) The autoxidation mechanism driven by Criegee Intermediates (CI).[13]

There is recent evidence, however, for an additional autoxidation mechanism initiated not by H-abstraction but rather by direct OH addition to the C=C bond(s) of an alkene, as illustrated in Fig. 1B. In this case the key intermediate is still a peroxy radical albeit functionalized with a hydroxyl group on the carbon atom adjacent (*i.e.,* in the beta position) to the $RO_2^\bullet$ group (β-hydroxy peroxy radical, β-OH-$RO_2^\bullet$). Beauchamp and coworkers[3, 14, 15] first reported compelling evidence, during the oxidation of lipids by OH radicals, for the formation of Criegee intermediates (CI), which they attributed to a unimolecular scission reaction of β-OH-$RO_2^\bullet$. Later, Wilson and coworkers[13] examined the heterogeneous reactions of OH with alkene nanoparticles and detected distinctive reaction products such as secondary ozonides (SOZ) that are formed solely by CI. Using CI scavengers (*e.g.,* alcohols) they were able to attenuate the autoxidation rate suggesting that CI are central for maintaining the radical pool and propagating the radical chain reactions. The

propagation step likely occurs through the unimolecular decomposition of CI to re-form OH radicals; a pathway that is well established in the gas phase.[16, 17]

A key uncertainty in these studies is exact pathway(s) by which CI are formed from β-OH-RO$_2$•. In the studies first by Beauchamp,[3, 14, 15] and then by Wilson[13] and coworkers, this step is assumed to be direct and unimolecular. However, a computational study by Wagner[18] found that the unimolecular pathway is energetically unfavorable. Instead, he proposed an alternative bimolecular mechanism and showed that CI could be produced in a reaction between two β-OH-RO$_2$• radicals mediated by an intermolecular H-shift.[18] Currently, it remains highly uncertain as to how CI are formed from β-OH-RO$_2$• and whether this transformation requires the solvated environment of the condensed phase or whether there are analogous pathways in the gas phase.[13, 15, 18, 19]

Here, we aim to ascertain the kinetic viability of various unimolecular and bimolecular reaction pathways that could plausibly connect β-OH-RO$_2$• with CI. To do this we first measure the heterogeneous reaction kinetics of OH with a model compound containing six C=C bonds: squalene (Sqe); a major lipid (~ 12%) in human sebum.[20] The evolution of Sqe and its major products are recorded as a function of reaction time and as a function of [OH]. From the decay kinetics of Sqe, effective uptake kinetics are computed. As shown previously,[13, 21] effective uptake coefficients (γ_{eff}) are sensitive to the extent of particle-phase radical chain reactions. Large effective uptake coefficients ($\gamma_{eff} \gg 1$) indicate extensive chain cycling, whereas reaction rates that proceed at or near the OH-particle collision limit ($\gamma_{eff} \sim 1$) do not. This experimental data set serves as an experimental benchmark for evaluating the possible mechanistic pathways that link the formation of CI from β-OH-RO$_2$• radical implemented in a kinetic model. The kinetic models are intended to be predictive, so the autoxidation mechanisms are constructed using realistic rate

coefficients where possible using elementary reactions based on previous literature.[13-15, 18] Three model scenarios are considered, 1 unimolecular and 2 bimolecular pathways, in order to identify which of mechanisms proposed to date are the most feasible autoxidation pathway to explain the observed multiphase kinetics of OH and Sqe.

2. MATERIALS AND METHODS

2.1. Experimental Details

Autoxidation kinetics are measured heterogeneously, where gas-phase OH radicals (produced by photolysis) are allowed to collide and react with nanoparticles (i.e., aerosols) comprised of Sqe. The reaction is conducted in a continuous flow stirred tank reactor (CFSTR)[22] and the reaction kinetics are monitored using a vacuum ultraviolet aerosol mass spectrometer (VUV-AMS).[23-25] This setup has been extensively detailed in prior publications,[13] thus only a brief description of the experimental setup is provided here.

Polydisperse Sqe aerosols are formed via a homogeneous nucleation by passing N_2 (0.3 standard liter per minute, SLM) through a heated Pyrex tube containing the liquid Sqe. The oven temperature is set at 135 ℃ to achieve stable particle formation. As the flow passes out of the cylindrical oven, it cools and nucleates submicron droplets ($\sim 10^6$ cm^{-3}) in a log-normal distribution with an average particle diameter $\sim$ 200 nm. The particle laden flow is then passed through an annular activated charcoal denuder to remove any residual gas-phase species produced during nucleation. Prior to entering the CFSTR, the particle flow is combined with additional flows containing the OH precursor (H_2O_2), N_2 and O_2 (0.1 SLM). H_2O_2 vapor is produced by passing N_2 (0.1 SLM) through a heated bubbler (60 ℃) containing equal mixtures of urea-hydroperoxide ($CO(NH_2)_2 \cdot H_2O_2$, Sigma-Aldrich, 97% pure) and sand (SiO_2, 50-70 mech particle size, Sigma-Aldrich). The final concentration of H_2O_2 in the CFSTR is less than 10 ppm and is measured by a

H_2O_2 sensor (Vaisala HPP272). An additional flow containing a gas-phase tracer (such as 2-methyl-2-butene, *n*-hexane or *n*-hexanal) is introduced into the CFSTR in order to determine the OH concentration using a mixed phase relative rate technique described in Refs. [13, 22] The final tracer concentration in the CFSTR is ~ 200 ppb. Measurements with and without the tracer show that it does not interfere with the overall chemistry. The total flow rate, including particles, N_2, O_2, tracer and H_2O_2, is ~ 1.1 SLM.

A measurement in the CFSTR occurs in three steps. First, prior to each experiment, the CFSTR is purged for hours with dry N_2 (~ 10 SLM) to eliminate particles, the tracer, H_2O_2, O_2 etc. from the previous experiment. Second, the CFSTR is filled with the fresh reagents (aerosols, H_2O_2, tracer, N_2 and O_2) with the photolysis lamps off (i.e., no reactions). The average particle mass concentration in the CFSTR is ~ 2000 $\mu g \cdot m^{-3}$ after ~ 2 hours of filling. To initiate the reaction, UV lamps (blacklights, $\lambda \sim 356$ nm, 45 cm in length) in the CFSTR are turned on to photolyze gas-phase H_2O_2 to produce OH. The UV lamps are housed inside 2.54 cm diameter GE type 214 quartz sleeves. The concentration of OH radicals is controlled by adjusting the power supplied to the UV lamps using a Variac.

The reaction mixture exiting the CFSTR is monitored by three instruments. A gas chromatograph, equipped with a flame ionization detector (GC-FID, SRI Instruments 8610C), is used to quantify the gas-phase tracer concentration in order to compute the average concentration of OH radicals in the CFSTR.[13, 22] A scanning mobility particle sizer (SMPS, TSI 3080L DMA and 3025A CPC) is used to measure the particle size distribution. Lastly, the chemical composition of the aerosol is measured using the VUV-AMS at the Chemical Dynamics Beamline (9.0.2), located at the Advanced Light Source, Lawrence Berkeley National Laboratory, Berkeley, CA, USA. The VUV light is filtered by an Argon gas filter and a MgF_2 window to remove the high

energy harmonics produced by the undulator. Aerosol mass spectra are collected by first vaporizing the particles at ~ 130 °C and then photoionizing the gas-phase components at a photon energy of 9.6 eV. During the vaporization process, the aerosols beam hits a copper block, located in the ionization region in the mass spectrometer, which is heated to flash vaporize the aerosols particles into gas phase components. This energy is used to minimize ion fragmentation. This instrument has been used extensively in prior studies of aerosols undergoing heterogeneous reactions.[23-28]

2.2. Construction of Autoxidation Mechanisms

Autoxidation consists of free radical chain reactions, which occur in three stages: initiation, propagation, and termination. As discussed above, recent experimental studies observed unusual secondary ozonides (SOZs) products,[26] that could not be easily explained by established autoxidation or peroxidation mechanisms.[11, 12] Instead, Beauchamp and coworkers[14, 15] found compelling evidence that CI are produced from the reactions of lipids with OH radicals. Zeng et al.[13] further demonstrated that bimolecular reactions of CI with aldehydes could explain the formation of SOZs, and that the unimolecular reactions of CI to regenerate OH radicals could sustain autoxidation. Thus, we consider three autoxidation scenarios that are driven by reactions of CI. These scenarios are illustrated in Fig. 2. Additional details for these three scenarios are shown in Figs. S1-S3 and Table S1 in the *Supporting Information*.

Scenario 1 is based on the original observations of Beauchamp and coworkers[15] and later by the explicit autoxidation mechanism proposed by Zeng et al.[13] In this scenario, gas-phase OH radicals adsorb to the surface of an aerosol and then add to the C=C bond(s) of Sqe (R1 in Fig. 2). This creates a β-hydroxy alkyl radical (β-OH-R•), which upon O_2 addition generates a β-hydroxy peroxy radical (β-OH-RO$_2$•, R2). Then, as proposed by Beauchamp and coworkers,[14, 15]

unimolecular C-C bond scission of β-OH-RO$_2{}^\bullet$ directly forms the CI and an α-hydroxy alkyl radical (α-OH-R$^\bullet$) coproduct (R3). The bimolecular reaction of α-OH-R$^\bullet$ with O$_2$ generates aldehyde and HO$_2$ radical. Once the CI is formed, its unimolecular decomposition regenerates an OH radical (R4), a step that is widely observed in both the gas and condensed-phases. [16, 29, 30] The regeneration of a OH radical can go on to consume another Sqe molecule (see green line in Fig. 2), which maintains the radical pool and propagates the chain reaction leading to autoxidation. We also include other relevant reactions in Scenario 1 as shown in Table S1. These include bimolecular reactions of β-OH-RO$_2{}^\bullet$ radicals to generate the β-hydroxy alkoxy radical (β-OH-RO$^\bullet$, R12 in Table S1), reactions of β-OH-RO$^\bullet$ radical (R13 in Table S1), the reactions of CI with aldehydes to yield SOZs (R14 in Table S1), and further consumption pathways for aldehydes and SOZs (e.g., R15-R17 in Table S1).
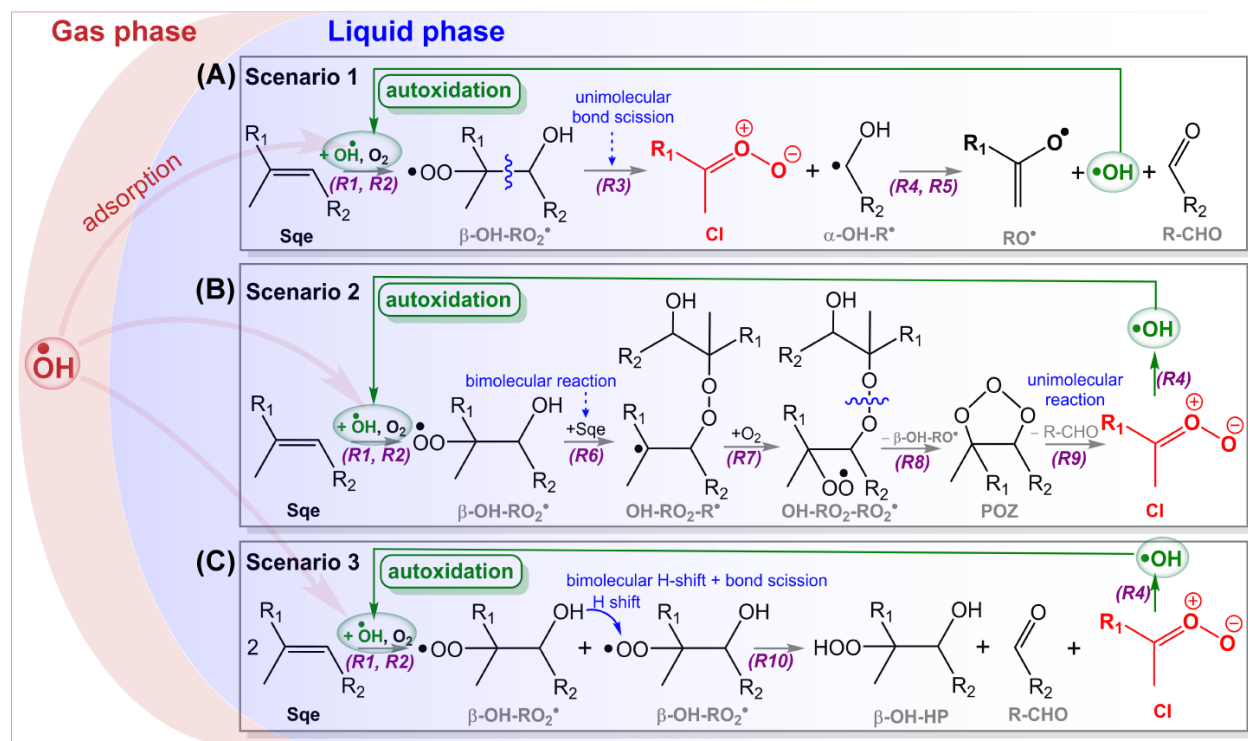
Figure 2. Three proposed scenarios that describe the heterogeneous autoxidation of squalene (Sqe) by OH radicals, which mainly include distinct formation pathways for CI and the OH regeneration reaction contributing to the autoxidation process. The reaction numbers are labelled under arrows.

Figure 2B illustrates the pathways included in Scenario 2. The initiation steps of adding OH to the C=C bond and subsequent O_2 addition to generate β-OH-RO$_2^\bullet$ radicals are same as those in Scenario 1. In contrast to Scenario 1, however, the β-OH-RO$_2^\bullet$ radical adds in a bimolecular step to the C=C bond of another Sqe molecule to produce an oxygenated alkyl radical (OH-RO$_2$-R$^\bullet$, R6). Peroxy radical addition to C=C double bonds in alkenes is well-documented.[1, 5, 31] The second O_2 addition to OH-RO$_2$-R$^\bullet$ generates a peroxy radical (OH-RO$_2$-RO$_2^\bullet$, R7).[31, 32] We hypothesize that O-O bond scission of OH-RO$_2$-RO$_2^\bullet$ could produce a primary ozonide (POZ, R8, Fig. 2B). As found in many ozonolysis studies,[27, 33-35] decomposition of the POZ generates a CI and aldehyde (R9). As in Scenario 1, the CI then regenerates OH, thus continuing the radical recycling process by consuming another Sqe molecule. In summary, Scenario 2 assumes that the CI is formed from the decomposition of a POZ, which itself is formed in a bimolecular reaction instead of the direct unimolecular route (i.e., β-OH-RO$_2^\bullet$ → CI) assumed in Scenario 1.

Figure 2C shows the autoxidation mechanism of Scenario 3. The initiation steps from Sqe to generate the β-OH-RO$_2^\bullet$ radical are identical to those in Scenarios 1 and 2. This scenario is the mechanism proposed by Wagner[18], whereby two β-OH-RO$_2^\bullet$ radicals undergo a bimolecular self-reaction to generate a CI, an aldehyde and a β-hydroxy hydroperoxide product (R10, Fig. 2C). This self-reaction proceeds via an internal H shift. OH regeneration from the CI and its role in driving the autoxidation process in Scenario 3 is identical to those in Scenarios 1 and 2.

2.3. Simulation Method

Kinetic simulations of the three mechanistic scenarios are conducted in Kinetiscope©,[36] which has been used extensively to model heterogeneous reactions.[27, 37-41] A single instantaneously mixed compartment is used to represent the Sqe aerosol, which is a valid assumption for a liquid that is well-mixed on reaction timescales. To properly account for surface-to-volume scaling of a spherical aerosol with radius, R, single rectangular prism compartment of dimensions 1 nm × 1 nm × (R/3) nm is used as described previously by Houle and coworkers.[27, 40, 42] The kinetic model is comprised of three parts: (a) the adsorption of gas-phase OH onto the surface of the Sqe aerosol, which occurs in a 1 nm thick surface region; (b) condensed-phase chemical reactions; and (c) evaporation of volatile products, such as the volatile ketones and aldehydes. Additional details for representing the adsorption and evaporation steps in such a kinetic model can be found in previous work.[27, 37-41] The condensed-phase chemical reactions and rate constants for these three scenarios are listed in Table S1 in the *Supporting Information*.

3. RESULTS AND DISCUSSION

Three kinds of experimental data are measured and used to quantitatively evaluate the three mechanistic scenarios described above. First, the decay kinetics of Sqe as a function of OH concentration are compared to scenario predictions. Second, the decay kinetics of Sqe are used determine how the effective reaction probability (γ_{eff}) of Sqe scales with [OH]. γ_{eff}, the fraction of gas-phase OH collisions that yield a Sqe reaction, is a sensitive metric for the degree of radical chain cycling in a heterogeneous reaction.[13, 22] For example, if Sqe is consumed at a rate that matches the OH collision frequency, then $\gamma_{eff} = 1$. Alternatively, signatures of radical chain reactions and autoxidation are obtained when the consumption rate of Sqe exceeds the OH collision frequency (i.e., $\gamma_{eff} > 1$), which is a clear indicator of additional radical consumption pathways beyond gas-phase OH.[13] Third, the kinetics of the major products are measured and

compared to scenario predictions. To do this product abundances (%) relative to the unreacted Sqe are compared to scenario predictions.

3.1. Role of Criegee Intermediates in the Heterogeneous Autoxidation

Figures 3A to 3C show the decay kinetics of Sqe as a function of residence time and [OH] ranging from 6.8×10^5 to 1.55×10^7 molec.·cm^{-3}. This OH concentration range closely mimics the atmosphere as well as indoor environments and the potential contribution to the human oxidation field.[43] For comparison, predictions from Scenarios 1-3 are also shown in Fig. 3. Scenario 1 reasonably reproduces the evolution of Sqe, while Scenarios 2 and 3 significantly under-predict the decay rates of Sqe. As expected from this comparison, the simulated effective uptake coefficients (γ_{eff}) of Sqe for Scenario 1 more closely replicate the experimental values, as illustrated in Fig. 3D. In general, both experimental and simulated γ_{eff} are larger than 1, which means that secondary reactions dominate the kinetics (*i.e.,* autoxidation).[13] For example, at [OH] $\sim 6.8 \times 10^5$ molec.·cm^{-3}, γ_{eff} approaches ~ 70 indicating that for every OH collision, 70 Sqe molecules are consumed in chain reactions. Moreover, γ_{eff} decreases as the [OH] increases, which provides an important clue for the reaction mechanism as will be described below.
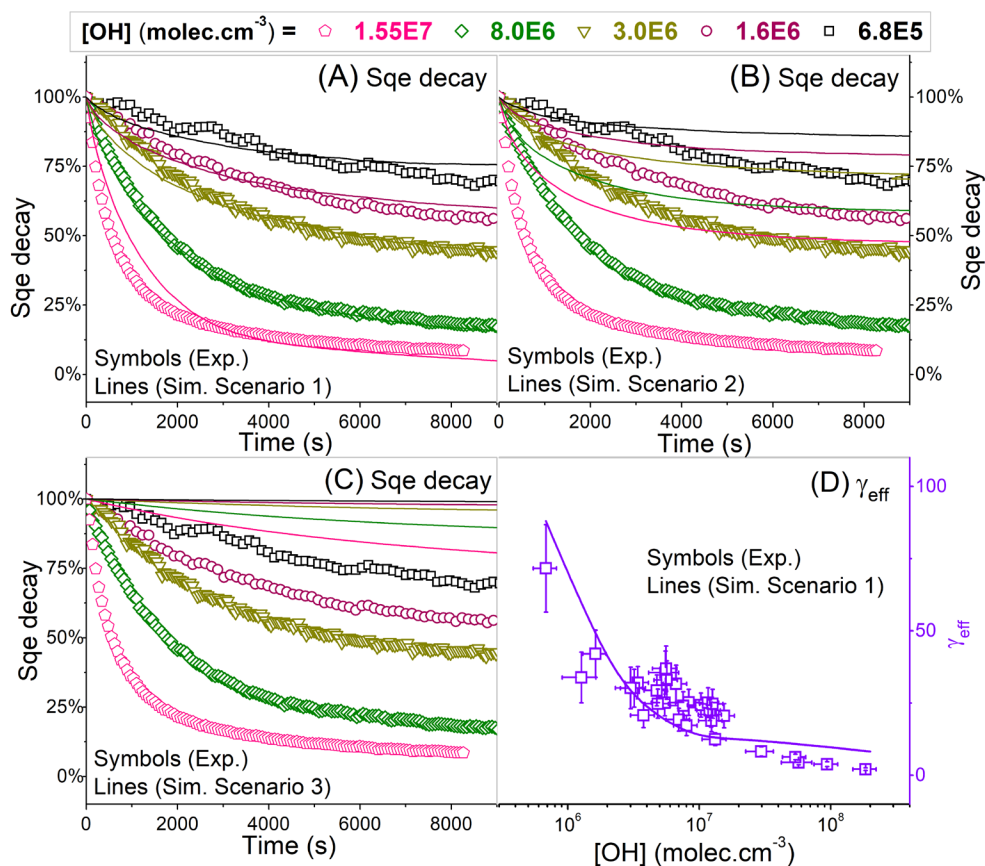
Figure 3. (A-C) The experimental (symbols) and simulated (lines) decay of Sqe as a function of residence time and [OH] (molec.·cm^{-3}). Simulations by Scenarios 1, 2, and 3 are shown in (A), (B) and (C), respectively. (D) Experimental (symbols)[13] and simulated (line, Scenario 1) effective reaction probability (γ_{eff}) of Sqe as a function of [OH].

Since all three scenarios assume the same propagation step, which is the unimolecular decomposition of the CI to regenerate OH radicals, the main difference in these three mechanisms lies in how CI form. The scaling of γ_{eff} with [OH] shown in Fig. 3D and captured by Scenario 1 arises from the facile competition between radical termination reactions favored at high [OH] vs. radical propagation, which dominates at low [OH]. The main radical termination step in Scenario 1 occurs via the β-OH-RO$_2$• + β-OH-RO$_2$• self-reaction (R12 in Table S1). The rate of this termination step scales as the square of the peroxy radical concentration, which increases with increasing [OH]. As the [OH] density decreases, the unimolecular propagation rate (β-OH-RO$_2$•

12

→ CI) increasingly outcompetes this bimolecular termination step leading to the scaling of γ_{eff} with [OH] observed in Fig. 3D.

This is in contrast with Scenario 3, in which CI are formed via the β-OH-RO$_2{}^\bullet$ bimolecular self-reaction. Thus, in Scenario 3, CIs should be favored when radical concentrations are high. An additional limitation for Scenario 3 is that two OH radicals react with 2 Sqe molecules to generate two β-OH-RO$_2{}^\bullet$ radicals, which in turn yields only one CI and therefore 1 OH radical. In other words, two OH radicals are consumed while only one OH radical is produced, which explains the failure of Scenario 3 to predict the observed autoxidation rate. Lastly, the inability of Scenario 2 to correctly predict the observed kinetics originates from the production of aldehydes associated with the formation pathways leading up to the formation of the POZ, the CI precursor. One cycle of oxidation in Scenario 2 to a produce a single CI also forms 3 aldehydes, which is shown explicitly in Fig. S2. The production of so many aldehydes rapidly consume the CI to form SOZ (a termination pathway) thus effectively shutting down the regeneration of OH from the unimolecular decomposition of CI (R4, Fig. 2B).

Although Scenario 1 can reasonably explain the overall Sqe autoxidation kinetics, the unimolecular reaction, β-OH-RO$_2{}^\bullet$ → CI, remains highly uncertain. Zhang *et al.*[15] calculated the energy barrier for this reaction to be high (~ 2.11 eV). Their calculation assumed a small, isolated CI in the gas phase and speculated that this substantial barrier could be reduced in the condensed phase due to clustering of molecules such as water with the transition state. Wagner's[18] theoretical analysis largely agrees with this conclusion that the unimolecular pathway would be energetically unfavorable.

In our previous work,[26] we reported evidence for the existence of OH chemistry during the heterogeneous oxidation of *cis*-9-tricosene (Tri) aerosols with gas-phase O$_3$. In this system the CI

is directly formed via reactions of O_3 with Tri, which then produces OH radical recycling. The rate constant for the assumed unimolecular scission reaction of β-OH-RO$_2^\bullet$ → CI was estimated to be 120 s^{-1}, which is constrained by the experimental kinetics.[26] This is the rate constant assumed in Scenario 1. As expected, the overall model predictions are sensitive to magnitude of this rate constant, which is illustrated in Fig. 4 with test models that assume a 10 times faster (1200 s^{-1}) and a 10 times slower rate constant (12 s^{-1}). This comparison clearly shows that in Scenario 1 the rate limiting step for autoxidation is this rate of formation of CI from β-OH-RO$_2^\bullet$.
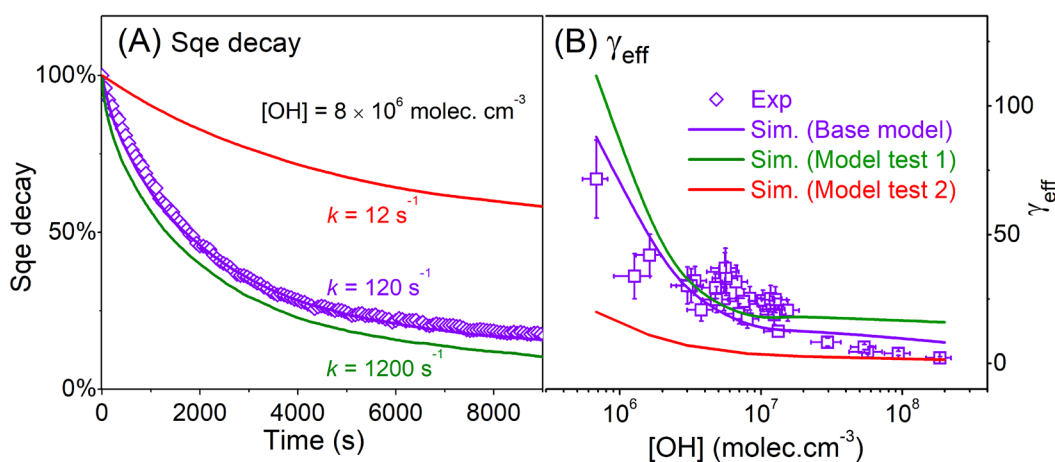


Figure 4. Experimental (symbols) and simulated (lines) (A) decay and (B) γ_{eff} of Sqe. Measured γ_{eff} values were reproduced from our previous work.[13] Simulations are from base model (Scenario 1), test model 1 and test model 2 by modifying rate constants of the unimolecular reaction of β-OH-RO$_2^\bullet$ to generate CI (R3).

3.2. The Evolution of Aldehydes

Figure 5A is an aerosol mass spectrum, reproduced from our previous work,[13] recorded during the heterogeneous reaction of Sqe with gaseous OH radicals. Products peaks at m/z = 248, 316 and 384 are aldehydes ($C_{17}H_{28}O$, $C_{22}H_{36}O$ and $C_{27}H_{44}O$), while products at m/z = 322, 390, 458, 526 and 594 are assigned to C_{20}, C_{25}, C_{30}, C_{35} and C_{40} secondary ozonides (SOZs) (i.e., $C_{20}H_{34}O_3$, $C_{25}H_{42}O_3$, $C_{30}H_{50}O_3$, $C_{35}H_{58}O_3$ and $C_{40}H_{66}O_3$). These aldehydes and SOZs are nearly identical to

those products observed in heterogeneous ozonolysis of Sqe.[27] Aldehydes and SOZs are prototypical products observed in ozonolysis reactions.[27, 34, 44-47] The formation kinetics of these major products provide additional constraints for the model scenarios described above.
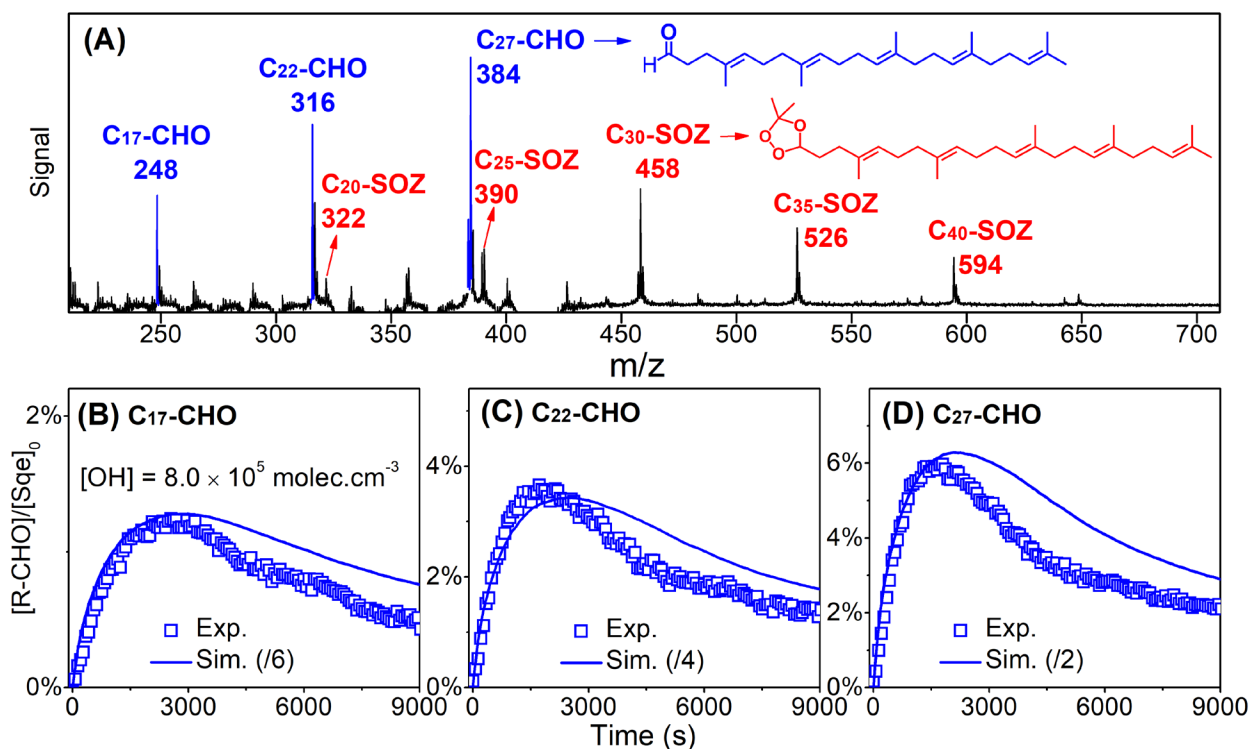

Figure 5. (A) Difference mass spectra (unreacted Sqe – reacted Sqe) of the OH + Sqe reaction products showing three aldehyde products (R-CHO, blue) and five secondary ozonides (SOZs, red). Chemical structures for representative isomers are presented. (B-D) Experimental (symbols) and simulated (lines) aldehyde kinetics. Simulations by Scenario 1 were divided factors when comparing with the experimental values.

The exact formation pathways for aldehydes are shown in Figs. S1-S3 in the *Supporting Information*. Sqe has three distinct C=C bonds, which upon OH and subsequent O_2 addition yield structurally distinct β-OH-$RO_2^\bullet$. In Scenario 1, unimolecular reactions of these β-OH-$RO_2^\bullet$ radicals generate CI and α-hydroxy alkyl radicals (α-OH-$R^\bullet$) with distinct carbon numbers.

Further reactions of α-OH-R$^{\bullet}$ radicals produce aldehydes, i.e., $C_{27}H_{44}O$, $C_{22}H_{36}O$ and $C_{17}H_{28}O$. These unsaturated aldehydes are consumed by OH as well as by reactions with CI to form SOZs. As shown in Fig. 5, Scenario 1 can reasonably reproduce the observed kinetics of the three major aldehyde products. Due to the lack of photoionization cross-sections and ion fragmentation patterns, it is difficult to compare absolute abundance of these aldehydes. Thus, the simulations are compared with experiment using a scaling factor.

The C_{27} aldehyde kinetics as a function of [OH] is compared to the predictions of Scenarios 1-3 in Fig. 6. Scenario 1 captures the experimental trend with [OH]. For example, the experimental and simulated peak value of the C_{27} aldehyde shifts to longer residence time under lower [OH]. This is because the aldehyde is mainly consumed via its reaction with OH radical, which contributes much less at lower [OH]. Meanwhile, the simulated concentrations of C_{27} aldehyde in Scenarios 2 and 3 predict formation kinetics of the aldehydes, which are too slow relative to the experimental observations. This is consistent with the slow Sqe decay rate for these Scenarios as illustrated in Fig. 3.


16
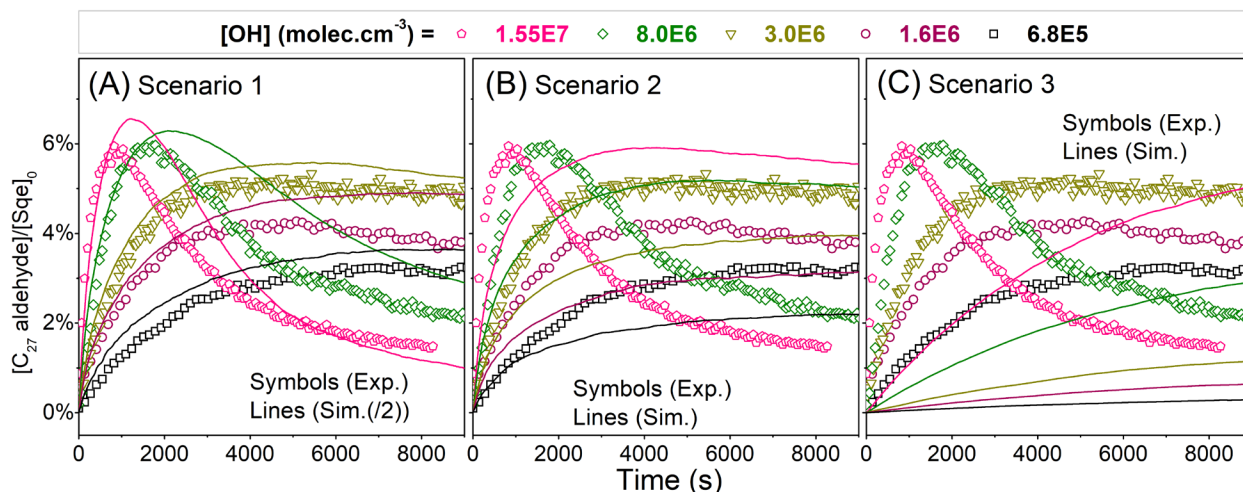
Figure 6. Experimental (symbols) and simulated (lines) results of C_{27} aldehyde ($C_{27}H_{44}O$, C_{27}-CHO) as a function of residence time and [OH] for (A) Scenario 1, (B) Scenario 2 and (C) Scenario 3.

Since the consumption pathways for aldehydes in all three scenarios are the same, the deviations observed in Scenarios 2 and 3 come from differences in the aldehyde formation mechanisms. In Scenario 2, aldehydes accompany the formation of the CI upon the unimolecular decomposition of the primary ozonide (POZ). In Scenario 3, the aldehyde and CI are both produced in the bimolecular reaction of two β-OH-RO$_2$• radicals. The slow aldehyde formation kinetics predicted in Scenarios 2 and 3 are consistent with the overall slow autoxidation rate, which is driven by the OH regeneration from the unimolecular reaction of CI.

3.3. The Evolution of Secondary Ozonides

Secondary ozonides (SOZs) are recognized to be characteristic products generated during the ozonolysis of unsaturated molecules.[33] Our previous work[13] observed, unexpectedly, peaks in the aerosol mass spectrum that corresponding to SOZs, formed not during ozonolysis but rather during OH heterogeneous reactions with Sqe. To further evaluate the present autoxidation mechanisms, the concentrations of SOZs as a function of residence time are measured in this work and shown in Fig. 7. The concentrations of C_{30} and C_{35} SOZs as a function of residence time are compared only to Scenario 1 since Scenarios 2 and 3 are unable to adequately explain the Sqe decay kinetics and the formation rate of the aldehyde products as discussed above. Figure 7 clearly illustrates that the measured peak concentrations of the SOZs appear at a much earlier residence time ($t \sim 1650$ s) than the simulations ($t \sim 3400$ s).

17
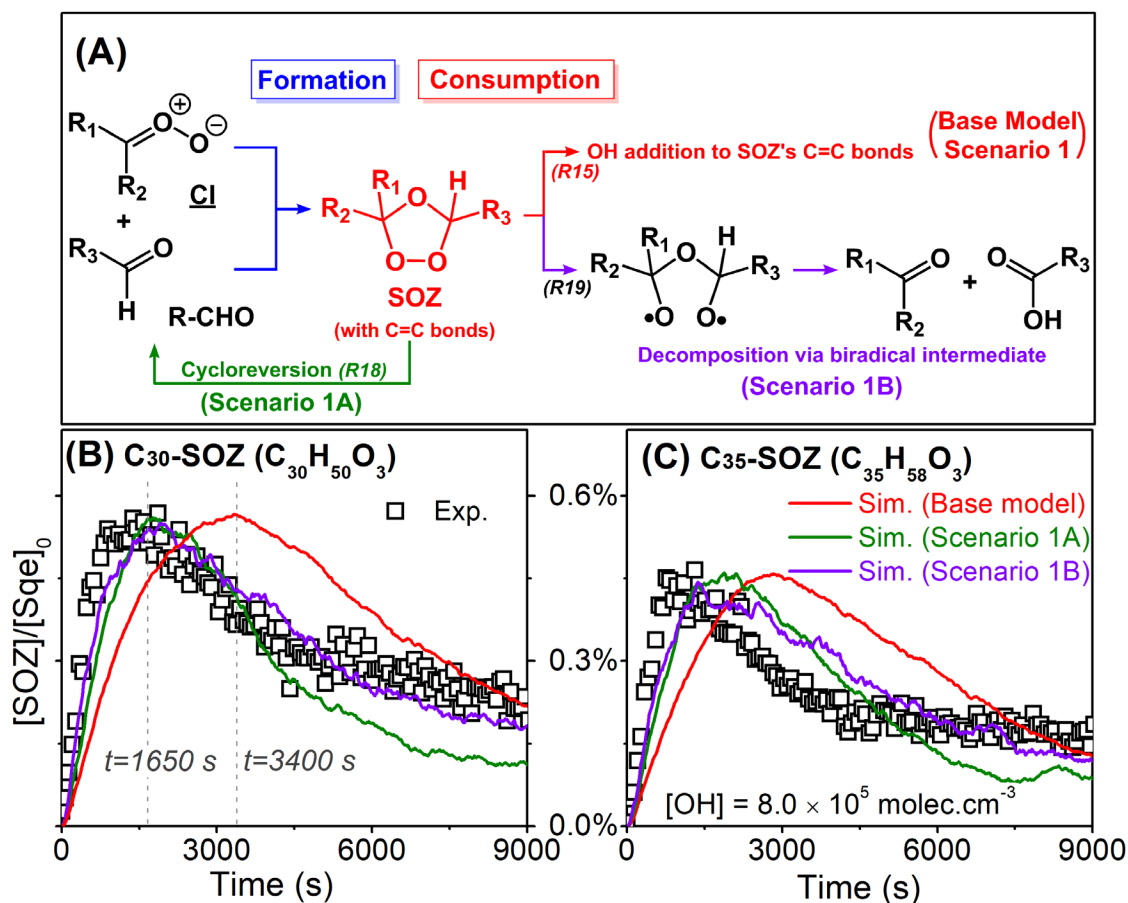
Figure 7. (A) The formation and consumption pathways of SOZ. (B and C) Experimental (symbols) and simulated (solid lines) concentrations of C_{30} and C_{35} SOZs. Simulations are predicted by the base model (Scenario 1), Scenario 1A and Scenario 1B.

This disagreement between the measured and predicted SOZ is similar to that reported in previous heterogeneous reactions of O_3 with unsaturated molecules.[27, 48] For example, Karagulian et al.[48] investigated the heterogeneous ozonolysis of 1-oleoyl-2-palmitoyl-sn-glycero-3-phosphocholine (OPPC). They found that the conventional mechanism for SOZ formation, the reaction of a CI with an aldehyde, was insufficient to quantitatively explain the SOZ formation kinetics in this system. A new formation pathway was proposed by Karagulian et al., in which SOZ could be formed via a direct reaction of O_3 with the POZ (i.e., POZ + $O_3 \rightarrow$ SOZ). Similarly, Heine et al.[27] reported a similar disagreement between the experimental and simulated evolution

of SOZs in ozonolysis of Sqe. Both studies suggest that there are additional formation pathways for SOZ beyond the conventional CI + aldehyde reaction.

We attempted to improve the predictions of Scenario 1 by considering additional sources and sinks for SOZ. The mechanism proposed by Karagulian et al.[48] for the formation of SOZ from O_3 + POZ is not applicable, since O_3 is not present in our reactor. Ellis et al.[49] investigated the gas-phase consumption reactions of ionized lipid ozonides and proposed several new consumption pathways that are activated by collisions or by near UV photons (e.g. $\lambda = 300$ nm), both of which are present in our reactor. First, they observed evidence for a SOZ cycloreversion reaction back to a CI and an aldehyde. The second mechanism involves O-O bond cleavage of the SOZ to generate a biradical. The rearrangement of this biradical then forms a carboxylic acid + aldehyde via 1,4-H shift, or an ester + acid via 1,4-alkyl shift. A beta-scission of this biradical could also generate an acid anhydride + byproduct, such as alkane and ester. Since we find no experimental evidence for the formation of an acid anhydride or ester in present experiments, we consider only the cycloreversion and biradical pathways proposed by Ellis et al.[49] as shown in Fig. 7A.

Scenario 1A is used to evaluate the importance of the cycloreversion reaction for predicting SOZ kinetics. Scenario 1A has all of the same pathways of Scenario 1, but includes an additional sink (i.e., SOZ $\rightarrow$ CI + aldehyde). As illustrated in Fig. 7, the peak [SOZ] predicted by Scenario 1A shifts to shorter reaction times, producing a more favorable comparison with experiments than Scenario 1 (i.e., base model). The decomposition reaction of the SOZ to form a biradical,[49] which further generates aldehyde and acid, is also tested. The biradical is expected to be highly reactive and short lived and thus we don't expect to be able to observe it experimentally. Scenario 1B adds this SOZ sink to Scenario 1. As illustrated in Fig. 7, Scenario 1B more closely replicates the

experimental SOZ kinetics. The rate constants for the cycloreversion reaction and lumped reactions of SOZs are estimated here and shown in Table S1.

4. ATMOSPHERIC IMPLICATIONS

In this work, we report direct evidence for the autoxidation of unsaturated organic aerosols upon the exposure of OH radicals. Although previous experimental results reveal the importance of CI in driving the autoxidation process,[13] the exact formation pathways of CI in OH initiated reactions remains highly uncertain.[13-15, 18] This mechanistic uncertainty limits our molecular understanding of pathways that lead to oxidative stress or the degradation rate of organic molecules in aerosol. To address this uncertainty, three plausible autoxidation mechanisms are tested quantitatively. These scenarios incorporate different formation mechanisms for CI and are evaluated against the experimentally measured heterogeneous kinetics of OH and Sqe. This comparison suggests that Scenario 1, where unimolecular C-C bond scission of β-OH-RO$_2^\bullet$ generates a CI, is the most kinetically viable, whereas Scenarios 2 and 3, which assume bimolecular reactions of β-OH-RO$_2^\bullet$ to produce CI, predict kinetics that are much too slow. Scenario 1 also makes reasonable predictions of the product formation kinetics of the major species (aldehydes and SOZ) produced in autoxidation of Sqe. Further, theoretical work is needed to clarify the mechanistic pathways that connect β-OH-RO$_2^\bullet$ and CI, especially since theory to date indicates that the barrier for a unimolecular pathway is quite high. This work further highlights the close mechanistic connection between important oxidants ($^\bullet$OH, RO$_2^\bullet$ and CI) in the environment, which have previously thought to react and participate in rather different oxidation mechanisms. Considering the contribution of present autoxidation mechanism to a variety of processes that affect human health, food storage, atmospheric environment etc., other organic molecules that

react with CI need to be considered, such as water and carboxylic acids, since these molecules are CI scavenger.

ASSOCIATED CONTENT

Supporting Information.

Additional details for the autoxidation mechanisms. Table S1 lists the reactions and their rate constants used in Scenarios 1, 2 and 3. Figures S1-S3 present representative reaction schemes proposed in three scenarios.

AUTHOR INFORMATION

Corresponding Author

Kevin R. Wilson – *Chemical Sciences Division, Lawrence Berkeley National Laboratory, Berkeley, CA 94720, United States;* orcid.org/0000-0003-0264-0872; Email: kwilson@lbl.gov

Author

Meirong Zeng – *College of Smart Energy, Shanghai Jiao Tong University, Shanghai 200240, PR China;* orcid.org/0000-0003-3902-7430; Email: meirongzeng@sjtu.edu.cn

Notes

The authors declare no competing financial interest.

ACKNOWLEDGMENTS

REFERENCES

1.   Yin, H.; Xu, L.; Porter, N. A., Free radical lipid peroxidation: mechanisms and analysis. *Chem. Rev.* **2011,** *111*, (10), 5944-5972.

2.   Yang, B.; Chen, Y.; Shi, J., Reactive Oxygen Species (ROS)-Based Nanomedicine. *Chem. Rev.* **2019,** *119*, (8), 4881-4985.

3.   Zhang, X.; Barraza, K. M.; Upton, K. T.; Beauchamp, J. L., Time resolved study of hydroxyl radical oxidation of oleic acid at the air-water interface. *Chem. Phys. Lett.* **2017,** *683*, 76-82.

4.   Gaschler, M. M.; Stockwell, B. R., Lipid peroxidation in cell death. *Biochem. Biophys. Res. Commun.* **2017,** *482*, (3), 419-425.

5.   Schaich, K. M., Analysis of Lipid and Protein Oxidation in Fats, Oils, and Foods. In *Oxidative stability and shelf life of foods containing oils and fats*, AOCS Press: 2016; pp 1-131.

6.   Pöschl, U.; Shiraiwa, M., Multiphase chemistry at the atmosphere-biosphere interface influencing climate and public health in the anthropocene. *Chem. Rev.* **2015,** *115*, (10), 4440-4475.

7.   Zhang, W.; Zhao, Z.; Shen, C.; Zhang, H., Unexpectedly Efficient Aging of Organic Aerosols Mediated by Autoxidation. *Environ. Sci. Technol.* **2023,** *57*, (17), 6965-6974.

8.   Herrmann, H.; Schaefer, T.; Tilgner, A.; Styler, S. A.; Weller, C.; Teich, M.; Otto, T., Tropospheric aqueous-phase chemistry: kinetics, mechanisms, and its coupling to a changing gas phase. *Chem. Rev.* **2015,** *115*, (10), 4259-4334.

9.   Davidovits, P.; Kolb, C. E.; Williams, L. R.; Jayne, J. T.; Worsnop, D. R., Mass accommodation and chemical reactions at gas-liquid interfaces. *Chem. Rev.* **2006,** *106*, (4), 1323-1354.

10.   Gligorovski, S.; Strekowski, R.; Barbati, S.; Vione, D., Environmental implications of hydroxyl radicals (•OH). *Chem. Rev.* **2015,** *115*, (24), 13051-13092.

11.   Porter, N. A.; Weber, B. A.; Weenen, H.; Khan, J. A., Autoxidation of Polyunsaturated Lipids. Factors Controlling the Stereochemistry of Product Hydroperoxides. *J. Am. Chem. Soc.* **1980,** *102*, (17), 5597-5601.

12.   Porter, N. A.; Wujek, D. G., Autoxidation of Polyunsaturated Fatty Acids, an Expanded Mechanistic Study. *J. Am. Chem. Soc.* **1984,** *106*, (9), 2626-2629.

13.   Zeng, M.; Heine, N.; Wilson, K. R., Evidence that Criegee intermediates drive autoxidation in unsaturated lipids. *Proc. Natl. Acad. Sci. U. S. A.* **2020,** *117*, (9), 4486-4490.

14.   Zhang, X.; Barraza, K. M.; Upton, K. T.; Beauchamp, J. L., Subtle changes in lipid environment have profound effects on membrane oxidation chemistry. *J. Am. Chem. Soc.* **2018,** *140*, (50), 17492-17498.

15.   Zhang, X.; Barraza, K. M.; Beauchamp, J. L., Cholesterol provides nonsacrificial protection of membrane lipids from chemical damage at air-water interface. *Proc. Natl. Acad. Sci. U.S.A.* **2018,** *115*, (13), 3255-3260.

16.   Liu, F.; Beames, J. M.; Petit, A. S.; McCoy, A. B.; Lester, M. I., Infrared-driven unimolecular reaction of CH_3CHOO Criegee intermediates to OH radical products. *Science* **2014,** *345*, (6204), 1596-1598.

17.   Kidwell, N. M.; Li, H.; Wang, X.; Bowman, J. M.; Lester, M. I., Unimolecular dissociation dynamics of vibrationally activated CH_3CHOO Criegee intermediates to OH radical products. *Nat. Chem.* **2016,** *8*, (5), 509-514.

18.   Wagner, J. P., Criegee Intermediates in Autoxidation Reactions − Mechanistic Considerations. *J. Phys. Chem. A* **2021,** *125*, (1), 406-410.

19.   He, J.; Zhang, H.; Liu, Y.; Ju, Y.; He, Y.; Jiang, Y.; Jiang, J., Interfacial Extraction to Trap and Characterize the Criegee Intermediates from Phospholipid Ozonolysis. *Anal. Chem.* **2023,** *95*, (11), 5018-5023.

20.   Nicolaides, N., Skin lipids: their biochemical uniqueness. *Science* **1974,** *186*, (4158), 19-26.

21.   Richards-Henderson, N. K.; Goldstein, A. H.; Wilson, K. R., Large enhancement in the heterogeneous oxidation rate of organic aerosols by hydroxyl radicals in the presence of nitric oxide. *J. Phys. Chem. Lett.* **2015,** *6*, (22), 4451–4455.

22.   Che, D. L.; Smith, J. D.; Leone, S. R.; Ahmed, M.; Wilson, K. R., Quantifying the reactive uptake of OH by organic aerosols in a continuous flow stirred tank reactor. *Phys. Chem. Chem. Phys.* **2009,** *11*, (36), 7885-7895.

23.   Smith, J. D.; Kroll, J. H.; Cappa, C. D.; Che, D. L.; Liu, C. L.; Ahmed, M.; Leone, S. R.; Worsnop, D. R.; Wilson, K. R., The heterogeneous reaction of hydroxyl radicals with sub-micron squalane particles: a model system for understanding the oxidative aging of ambient aerosols. *Atmos. Chem. Phys.* **2009,** *9*, (9), 3209-3222.

24.   Wilson, K. R.; Jimenez-Cruz, M.; Nicolas, C.; Belau, L.; Leone, S. R.; Ahmed, M., Thermal vaporization of biological nanoparticles: fragment-free vacuum ultraviolet photoionization mass spectra of tryptophan, phenylalanine-glycine-glycine, and β-carotene. *J. Phys. Chem. A* **2006,** *110*, (6), 2106-2113.

25.   Wilson, K. R.; Peterka, D. S.; Jimenez-Cruz, M.; Leone, S. R.; Ahmed, M., VUV photoelectron imaging of biological nanoparticles: ionization energy determination of nanophase glycine and phenylalanine-glycine-glycine. *Phys. Chem. Chem. Phys.* **2006,** *8*, (16), 1884-1890.

26.   Zeng, M.; Wilson, K. R., Efficient Coupling of Reaction Pathways of Criegee Intermediates and Free Radicals in the Heterogeneous Ozonolysis of Alkenes. *J. Phys. Chem. Lett.* **2020,** *11*, (16), 6580-6585.

27.   Heine, N.; Houle, F. A.; Wilson, K. R., Connecting the elementary reaction pathways of Criegee intermediates to the chemical erosion of squalene interfaces during ozonolysis. *Environ. Sci. Technol.* **2017,** *51*, (23), 13740-13748.

28.   Richards-Henderson, N. K.; Goldstein, A. H.; Wilson, K. R., Sulfur dioxide accelerates the heterogeneous oxidation rate of organic aerosol by hydroxyl radicals. *Environ. Sci. Technol.* **2016,** *50*, (7), 3554-3561.

29.   Fang, Y.; Liu, F.; Barber, V. P.; Klippenstein, S. J.; McCoy, A. B.; Lester, M. I., Deep tunneling in the unimolecular decay of CH_3CHOO Criegee intermediates to OH radical products. *J. Chem. Phys.* **2016,** *145*, (23), 234308.

30.   Long, B.; Bao, J. L.; Truhlar, D. G., Atmospheric Chemistry of Criegee Intermediates: Unimolecular Reactions and Reactions with Water. *J. Am. Chem. Soc.* **2016,** *138*, (43), 14409-14422.

31.   Denisov, E. T.; Afanas'ev, I. B., *Oxidation and Antioxidants in Organic Chemistry and Biology.* Taylor & Frances: Oxford: 2005.

32.   Sun, H.; Bozzelli, J. W.; Law, C. K., Thermochemical and Kinetic Analysis on the Reactions of O_2 with Products from OH Addition to Isobutene, 2-Hydroxy-1,1-dimethylethyl, and 2-Hydroxy-2-methylpropyl Radicals: HO_2 Formation from Oxidation of Neopentane, Part II. *J. Phys. Chem. A* **2007,** *111*, (23), 4974-4986.

33.   Criegee, R., Mechanism of ozonolysis. *Angew. Chem. Int. Ed.* **1975,** *14*, (11), 745-752.

34.   Schwartz-Narbonne, H.; Wang, C.; Zhou, S.; Abbatt, J. P. D.; Faust, J., Heterogeneous Chlorination of Squalene and Oleic Acid. *Environ. Sci. Technol.* **2019,** *53*, (3), 1217-1224.

35.   Epstein, S. A.; Donahue, N. M., Ozonolysis of Cyclic Alkenes as Surrogates for Biogenic Terpenes: Primary Ozonide Formation and Decomposition. *J. Phys. Chem. A* **2010,** *114*, (28), 7509-7515.

36.   Hinsberg, W. D.; Houle, F. A. *Kineticscope* *https://hinsberg.net/kinetiscope/*, (accessed 2024-05-16)

37.   Houle, F. A.; Wiegel, A. A.; Wilson, K. R., Predicting aerosol reactivity across scales: from the laboratory to the atmosphere. *Environ. Sci. Technol.* **2018,** *52*, (23), 13774-13781.

38.   Houle, F. A.; Wiegel, A. A.; Wilson, K. R., Changes in reactivity as chemistry becomes confined to an interface. The case of free radical oxidation of $C_{30}H_{62}$ alkane by OH. *J. Phys. Chem. Lett.* **2018,** *9*, (5), 1053-1057.

39.   Wiegel, A. A.; Liu, M. J.; Hinsberg, W. D.; Wilson, K. R.; Houle, F. A., Diffusive confinement of free radical intermediates in the OH radical oxidation of semisolid aerosols. *Phys. Chem. Chem. Phys.* **2017,** *19*, (9), 6814-6830.

40.   Wiegel, A. A.; Wilson, K. R.; Hinsberg, W. D.; Houle, F. A., Stochastic methods for aerosol chemistry: a compact molecular description of functionalization and fragmentation in the heterogeneous oxidation of squalane aerosol by OH radicals. *Phys. Chem. Chem. Phys.* **2015,** *17*, (6), 4398-411.

41.   Houle, F. A.; Hinsberg, W. D.; Wilson, K. R., Oxidation of a model alkane aerosol by OH radical: the emergent nature of reactive uptake. *Phys. Chem. Chem. Phys.* **2015,** *17*, (6), 4412-4423.

42.   Heine, N.; Arata, C.; Goldstein, A. H.; Houle, F. A.; Wilson, K. R., Multiphase mechanism for the production of sulfuric acid from SO_2 by Criegee intermediates formed during the heterogeneous reaction of ozone with squalene. *J. Phys. Chem. Lett.* **2018,** *9*, (12), 3504-3510.

43.   Zannoni, N.; Lakey, P. S. J.; Won, Y.; Shiraiwa, M.; Rim, D.; Weschler, C. J.; Wang, N.; Ernle, L.; Li, M.; Bekö, G.; Wargocki, P.; Williams, J., The human oxidation field. *Science* **2022,** *377*, (6610), 1071-1077.

44.   Coffaro, B.; Weisel, C. P., Reactions and Products of Squalene and Ozone: A Review. *Environ. Sci. Technol.* **2022,** *56*, (12), 7396-7411.

45.   Arata, C.; Heine, N.; Wang, N.; Misztal, P. K.; Wargocki, P.; Beko, G.; Williams, J.; Nazaroff, W. W.; Wilson, K. R.; Goldstein, A. H., Heterogeneous Ozonolysis of Squalene: Gas-Phase Products Depend on Water Vapor Concentration. *Environ. Sci. Technol.* **2019,** *53*, (24), 14441-14448.

46.   Zhou, S.; Forbes, M. W.; Abbatt, J. P., Kinetics and products from heterogeneous oxidation of squalene with ozone. *Environ. Sci. Technol.* **2016,** *50*, (21), 11688-11697.

47.   Jacobs, M. I.; Xu, B.; Kostko, O.; Heine, N.; Ahmed, M.; Wilson, K. R., Probing the Heterogeneous Ozonolysis of Squalene Nanoparticles by Photoemission. *J. Phys. Chem. A* **2016,** *120*, (43), 8645-8656.

48.   Karagulian, F.; Scott Lea, A.; Dilbeck, C. W.; Finlayson-Pitts, B. J., A new mechanism for ozonolysis of unsaturated organics on solids: phosphocholines on NaCl as a model for sea salt particles. *Phys. Chem. Chem. Phys.* **2008,** *10*, (4), 528-541.

49.   Ellis, S. R.; Pham, H. T.; In Het Panhuis, M.; Trevitt, A. J.; Mitchell, T. W.; Blanksby, S. J., Radical Generation from the Gas-Phase Activation of Ionized Lipid Ozonides. *J. Am. Soc. Mass Spectrom* **2017,** *28*, (7), 1345-1358.

Table of Contents Graphic